Contribution from the Eastern Regional Research Center, USDA—ARS, 600 East Mermaid Lane, Philadelphia, Pennsylvania 19118, and Department of Chemistry and Materials Science Center, Cornell University, Ithaca, New York 14853

Isomorphous Substitution in Phyllosilicates as an Electronegativity Perturbation: Its Effect on Bonding and Charge Distribution

William F. Bleam*,† and Roald Hoffmann‡

Received November 10, 1987

Isomorphous substitution in 2:1 phyllosilicates is typified by the substitution of Si(IV) by Al(III) in the tetrahedral sheet and Al(III) by Mg(II) in the octahedral sheet. Qualitative perturbation theory and extended Hückel, tight-binding calculations show that most of the excess negative charge not remaining at the substitution site is deposited on nearest-neighbor oxygens in the Al(III) → Si(IV) case. Nearest-neighbor oxygens are bypassed and most of the displaced negative charge appears on next-nearest-neighbor aluminum atoms in the Mg(II) → Al(III) case. Next-nearest-neighbor interactions dominate when there are negligible orbital interactions between the nearest-neighbor oxygen atoms and the substituting atom. The electronegativity perturbation in the cases we studied causes the bonds in the polyhedra where the substitution occurs to lengthen, bonds in adjacent polyhedra to shorten, and the atomic populations to increase on the nearest- and next-nearest neighbor atoms.

Introduction

The negative charge on a phyllosilicate mineral (e.g., mica or smectite) layer results from isomorphous substitution of structural cations of higher valence by others with lower valence, e.g. Al(III) replacing Si(IV) in the tetrahedral sheet (viz., $Al(III)_{tet} \rightarrow Si(IV)_{tet}$) or Mg(II) replacing Al(III) in the octahedral sheet (viz., $Mg(II)_{oct} \rightarrow Al(III)_{oct}$). The excess negative charge is locally balanced by cations located *between* the layers. This phenomena is quite common in phyllosilicates where the ratio of tetrahedral sheets to octahedral sheets is 2:1 (Figure 1) and is an important property used in their classification.[1-4]

Mineralogists and chemists have long speculated on the distribution of excess negative charge arising from isomorphous substitution in phyllosilicates. According to Radoslovich,[5] the apical oxygens in celadonite, a mica with layer-charge arising from octahedral substitution of Al(III) by Mg(II), carry the excess negative charge. Sposito[6] suggests isomorphous substitution of tetrahedral Si(IV) by Al(III) deposits excess negative charge principally on the basal oxygens of the "siloxane ditrigonal" cavity, enhancing the Lewis base character of the cavity.

We have shown[7] the electronic structure of neutral-layer phyllosilicates can be viewed as essentially tetrahedral silicate sheets (Figure 2) perturbed by interactions with octahedral cations. We will indicate primitive cell stoichiometry and the two-dimensional, infinite topology of the tetrahedral sheets with the symbol ${}^2_\infty[Si_2O_5^{2-}]$. Given this, we can greatly simplify our investigation of tetrahedral substitution by examining *isolated* aluminosilicate tetrahedral sheets, ${}^2_\infty[Al_xSi_{2-x}O_5^{(2+x)-}]$. Our model for "octahedral-sheet" substitution will be $Mg(II)_{oct} \rightarrow Al(III)_{oct}$ and will rely on comparisons of pyrophyllite (${}^2_\infty[Al_2(OH)_2(Si_2O_5)_2]$) and celadonite ($K^+$, ${}^2_\infty[MgAl(OH)_2(Si_2O_5)_2^-]$).

All calculations were done with use of the extended Hückel, tight-binding method.[8-10] Considerable experience at the molecular level using extended Hückel theory allows us to distill a chemist's interpretation from the inherently delocalized nature of solid-state interactions. Details relevant to our calculations are found in the Appendix and Tables VI and VII.

† Eastern Research Center, USDA—ARS.
‡ Cornell University.

Bonding in Phyllosilicates

A picture of the electronic structure of silicates has emerged from the numerous quantum-chemical[11,12] and solid-state theoretical studies[13-15] over the years. The electronic states fall into two *groups* of bands, the "O(2p)" bands and the "O(2s)" bands. The uppermost occupied states are nonbonding (viz., "lone-pair" electron) states derived from O(2p) orbitals. States derived from interactions between Si(3p) and O(2p) orbitals are found at energies directly below the nonbonded O(2p) states. The stronger Si(3s)–O(2p) interactions lead to the states found at the bottom of the O(2p) group of bands. The energy range from the top of the O(2p) group of bands to the bottom is about 10 eV.[14,16-20] The

(1) Grim, R. E. *Clay Mineralogy*; McGraw-Hill: New York, 1968; p 34.
(2) van Olphen, H. *An Introduction to Clay Colloid Chemistry*; Wiley: New York, 1977; p 67.
(3) Brown, G.; Newmann, A. C. D.; Rayner, J. H.; Weir, A. H. In *The Chemistry of Soil Constituents*; Greenland, D. J., Hayes, M. H. B., Eds.; Wiley: New York, 1978; pp 29–178.
(4) Bailey, S. W. In *Crystal Structures of Clay Minerals and Their X-Ray Identification*; Brindley, G. W., Brown, G., Eds.; Mineralogical Society: London, 1980; pp 2–124.
(5) Radoslovich, E. W. *Am. Mineral.* **1963**, *48*, 76.
(6) Sposito, G. *The Surface Chemistry of Soils*; Oxford University Press: New York, 1984; p 15.
(7) Bleam, W.; Hoffmann, R. *Phys. Chem. Miner.*, in press.
(8) Hoffmann, R. *J. Chem. Phys.* **1963**, *39*, 1397.
(9) Hoffmann, R.; Lipscomb, W. N. *J. Chem. Phys.* **1962**, *36*, 2179.
(10) Whangbo, M.-H.; Hoffmann, R.; Woodward, R. B. *Proc. R. Soc. London, A* **1979**, *366*, 23.
(11) Tossell, J. A.; Gibbs, G. V. *Phys. Chem. Miner.* **1977**, *2*, 21.
(12) Gibbs, G. V. *Am. Mineral.* **1982**, *67*, 421.
(13) Griscom, D. L. *J. Non-Cryst. Solids* **1977**, *24*, 155.
(14) Pantelides, S. T. *Comments Solid State Phys.* **1977**, *8*, 55.
(15) Harrison, W. A. In *The Physics of SiO_2 and Its Interfaces*; Pantelides, S. T., Ed.; Pergamon: New York, 1978; pp 105–109.
(16) DiStefano, T. H.; Eastman, D. E. *Phys. Rev. Lett.* **1971**, *27*, 1560.
(17) Tossell, J. A.; Vaughan, D. J.; Johnson, K. H. *Chem. Phys. Lett.* **1973**, *20*, 329.
(18) Schneider, P. M.; Fowler, W. B. *Phys. Rev. Lett.* **1976**, *36*, 425.
(19) Schlüter, M.; Chelikowsky, J. R. *Solid State Comm.* **1977**, *21*, 381.

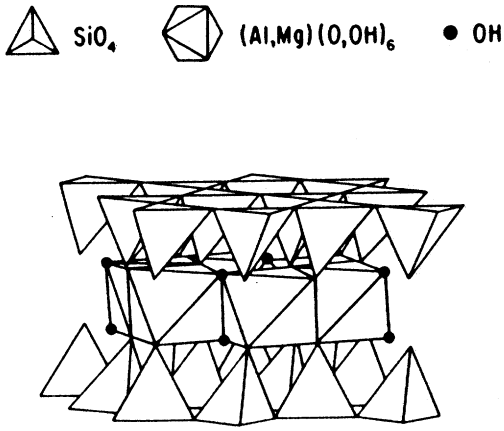

Figure 1. Polyhedra crystal structure of "2:1" phyllosilicates (the ratio of tetrahedral sheets to octahedral sheets is 2:1).

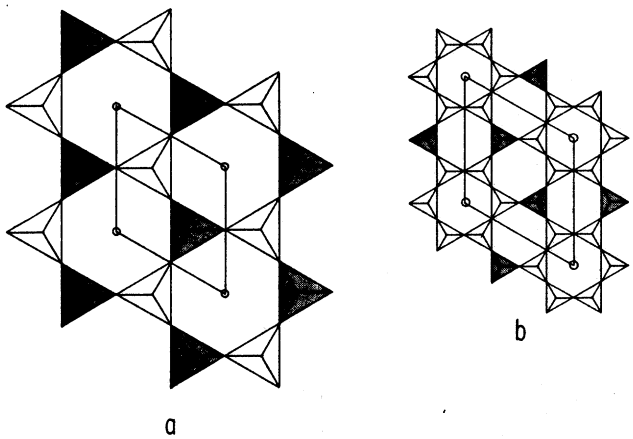

Figure 2. Tetrahedral sheets showing the primative cell: (a) ${}^{2}_{\infty}[AlSiO_5^{3-}]$ (layer group *p3m1*); (b) ${}^{2}_{\infty}[AlSi_3O_{10}^{5-}]$ (layer group *p6mm*).

uppermost states in the perturbed O(2s) group of bands are due to Si(3p)–O(2s) interactions. The lower portion of the O(2s) bands involves Si(3s)–O(2s) interactions. The O(2s) group of bands is about 5 eV wide.

White and Gibbs[22] found that the Si Kβ X-ray emission spectra (XES), involving the transition Si(1s) ← Si(3p), shows a positive correlation with the Al:Si ratio in aluminosilicates. Tossell et al.[17] attributed this to the destabilization of Si(3p) orbitals through mixing with higher energy Al(3p) orbitals. Tossell[23] assigned the Si Kβ' peak to transitions from states that are primarily *nonbonding* O(2s) states. Thus, the Kβ–Kβ' peak separation should increase when $Al(III)_{tet} \rightarrow Si(IV)_{tet}$ since nonbonding O(2s) states remain fixed while the bonding, [Al(3p),Si(3p)]–O(2p) states will be destabilized.

Gibbs et al.[24] used Mulliken overlap populations[25,26] to show that Si–O[–Al] should be a shorter, stronger bond than Si–O[–Si]. Several groups have examined $Al(III)_{tet} \rightarrow Si(IV)_{tet}$ in aluminosilicate framework structures using clusters as models for the solid state.[27–35] There is general agreement in these theoretical studies that the Q(Si), viz., the charge on silicon, is *less positive* in tetrahedra corner-sharing with aluminate tetrahedra. Oddly enough, some of these studies have $Q(O_{br}[-Al,-Si])$ *less* negative than $Q(O_{br}[(-Si)_2])$ (br = bridging), while others have it more negative.

Seyama and Soma[21] found systematic shifts in the photoelectron binding energies of Si, O, and Al in their study of charge redistribution in aluminosilicate minerals. Their results indicate an increase in electron density on both Si and O resulting from $Al(III)_{tet} \rightarrow Si(IV)_{tet}$ substitution in the framework.

Isomorphous Substitution as an Electronegativity Perturbation

I. Qualitative Analysis of Orbital Interactions in *p3m1* ${}^{2}_{\infty}[AlSiO_5^{3-}]$. Crystal structure carries valuable information about the dominant bonding mechanism. The "open", 4:2-coordination topology of SiO_2 is persuasive evidence that orbital interactions play a fundamental role in the structure and bonding of the various polymorphs of silica.[36–38] The perservation of this open framework structure in zeolites, feldspars, and the phyllosilicates assures us that $Al(III)_{tet} \rightarrow Si(IV)_{tet}$ does not subvert orbital interaction as a dominant bonding mechanism. There are, in fact, aluminates with 4:2-coordination topology. Such topologies are found in $NaAlO_2$ and $KAlO_2$, which have cristobalite-like structures,[39] and in $CaAl_2O_4$, a trydimite analogue.[40] Depmeier[41] shows that zeolitic structures were accessible to aluminate compounds, the mineral $Ca_8[Al_{12}O_{24}](WO_4)_2$ being a sodalite analogue. These examples clearly demonstrate a fundamental similarity of Si–O and Al–O bonds.

An electronegativity perturbation leaves a clear imprint on the orbital interactions in a molecule or solid. Quite simply, the atomic orbitals of the more electronegative atoms will make a greater contribution to the bonding orbitals than the less electronegative atoms. Conversely, the less electronegative element's atomic orbitals will have a larger contribution to the antibonding orbitals than the orbitals of more electronegative element. Since the less electronegative atom's orbitals lie at higher energies, the bonding orbitals will be destabilized by substituting such an element into the structure.[42–44] In very simple terms, the difference between a ${}^{2}_{\infty}[Si_2O_5^{2-}]$ tetrahedral sheet and a ${}^{2}_{\infty}[AlSiO_5^{3-}]$ sheet comes down to the orbital energies at the site occupied by the aluminum atom.

There are five oxygens, one aluminum, and one silicon per primitive cell in a ${}^{2}_{\infty}[AlSiO_5^{3-}]$ frame, giving a total of twenty-eight valence orbitals. To zeroth order in perturbation theory, we can imagine the occupied, valence bands as essentially oxygen states and the unoccupied, conduction bands as aluminum and silicon states. In the two-dimensional, infinite ${}^{2}_{\infty}[AlSiO_5^{3-}]$ sheet there will be twenty valence bands and eight conduction bands.

The twenty valence bands can be broadly classified in two ways. The valence bands arise from perturbed oxygen states in our qualitative picture; five are nominally "O(2s)" bands, and fifteen, "O(2p)" bands. Eight of the valence bands can be identified as "bonding" bands (all five of the O(2s) bands and three of the O(2p) bands), while the remaining twelve O(2p) bands are

(20) Dikov, Y. P.; Debolsky, E. I.; Romashenko, Y. N.; Dolin, S. P.; Levin, A. A. *Phys. Chem. Miner.* **1977**, *1*, 27.
(21) Seyama, H.; Soma, M. *J. Chem. Soc., Faraday Trans. 1* **1985**, *81*, 485.
(22) White, E. W.; Gibbs, G. V. *Am. Mineral.* **1967**, *52*, 985.
(23) Tossell, J. A. *J. Am. Chem. Soc.* **1975**, *97*, 4840.
(24) Gibbs, G. V.; Meagher, E. P.; Smith, J. V.; Pluth, J. J. In *Molecular Sieves II*; Katzer, J. R., Ed.; American Chemical Society: Washington, DC, 1977; pp 19–29.
(25) Mulliken, R. S. *J. Chem. Phys.* **1955**, *23*, 1833.
(26) Mulliken, R. S. *J. Chem. Phys.* **1955**, *23*, 2343.
(27) Beran, S.; Dubsky, J. *J. Phys. Chem.* **1979**, *83*, 2538.
(28) Mortier, W. J.; Geerlings, P.; van Alsenoy, C.; Figeys, H. P. *J. Phys. Chem.* **1979**, *83*, 855.
(29) Beran, S. *Z. Phys. Chem. (Munich)* **1980**, *123*, 129.
(30) Sauer, J.; Hobza, P.; Zahradnik, R. *J. Phys. Chem.* **1980**, *84*, 3318.
(31) De Jong, H. W. S.; Brown, G. E. *Geochim. Cosmochim. Acta* **1980**, *44*, 491.
(32) Hass, E. C.; Mezey, P. G.; Plath, P. J. *J. Mol. Struct.* **1981**, *76*, 389.
(33) Hass, E. C.; Mezey, P. G.; Plath, P. J. *J. Mol. Struct.* **1982**, *87*, 261.
(34) Beran, S. *Chem. Phys. Lett.* **1982**, *91*, 86.
(35) Derouane, E. G.; Fripiat, J. G. *Zeolites* **1985**, *5*, 165.
(36) Pantelides, S. T.; Harrison, W. A. *Phys. Rev. B: Solid State* **1976**, *13*, 2667.
(37) Harrison, W. A. In *Structure and Bonding in Crystals*; O'Keeffe, I. M., Narvrotsky, A., Eds.; Academic: New York, 1981; Vol. 1, pp 137–154.
(38) Harrison, W. A. *Electronic Structure and the Properties of Solids*; W. H. Freeman: San Francisco, CA, 1980; pp 43, 59–60.
(39) Barth, T. F. W. *J. Phys. Chem.* **1935**, *39*, 323.
(40) Hörkner, W.; Müller-Buschbaum, H. *J. Inorg. Nucl. Chem.* **1976**, *38*, 983.
(41) Depmeier, W. *Acta Crystallogr., Sect. C: Cryst. Struct. Commun.* **1984**, *40*, 226.
(42) Burdett, J. K.; McLarnan, T. *Am. Mineral*, **1984**, *69*, 601.
(43) Albright, T.; Burdett, J. K.; Whangbo, M.-H. *Orbital Interactions in Chemistry*; Wiley: New York, 1985; pp 229–257.
(44) Hoffmann, R. *Angew. Chem.*, in press.

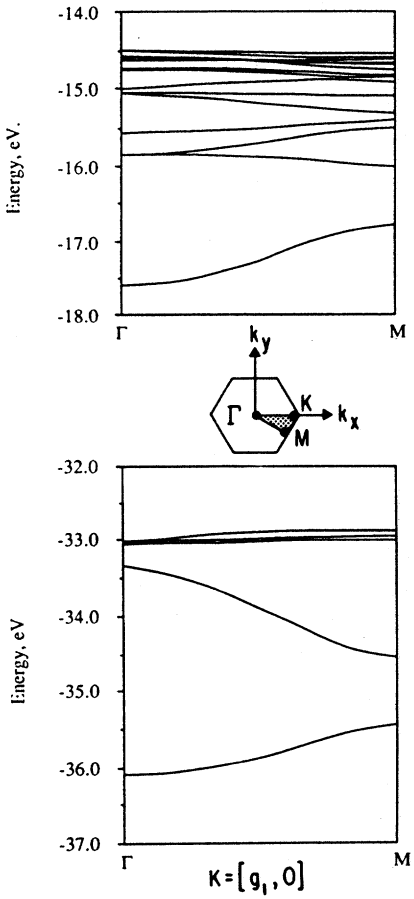

Figure 3. Band structure of the idealized $^2_\infty[Si_2O_5^{2-}]$ tetrahedral sheet (layer group *p6mm*) from $\mathbf{k}_\Gamma$ to $\mathbf{k}_M$ showing the first Brillouin zone with irreducible wedge (shaded), symmetry points, and lines.

"nonbonding". This qualitative, "eight-electron rule" analysis is completely in line with those developed in more detailed quantum-chemical and solid-state theoretical studies (vide infra).

II. Band Structure of Idealized Aluminosilicate Tetrahedral Sheets. The valence band structures for three different aluminosilicate tetrahedral sheets appear in Figures 3–5. The first of these, Figure 3, is for a $^2_\infty[Si_2O_5^{2-}]$ sheet composed of perfect silicate tetrahedra with Si–O bond lengths, *d*(Si–O), equal to 1.618 Å (see Appendix) and layer-group symmetry *p6mm*.[45]

The second, Figure 4, is for an idealized $^2_\infty[AlSiO_5^{3-}]$ sheet of perfect aluminate and silicate tetrahedra with tetrahedral bond lengths, *d*(T–O), of 1.618 Å and layer-group symmetry *p3m1*. This hypothetical tetrahedral sheet contains pseudo-aluminum atoms, **Al**. The exponents of the **Al**(3s) and **Al**(3p) orbitals match those used for the silicon orbitals (Table VI). Not only does *d*(Al–O) equal *d*(Si–O) in $^2_\infty[AlSiO_5^{3-}]$, but the pseudo-aluminum atom, **Al**, is the *same size* as the silicon atom.

We did this for a particular reason. When $Al(III)_{tet} \rightarrow Si(IV)_{tet}$, orbital interactions in the tetrahedral sheet are influenced by both (a) increased atomic size of the aluminum, the valence orbitals of aluminum being less tightly bound and more diffuse than those of silicon, and (b) the decreased electronegativity of aluminum. Our band-structure analysis of the idealized $^2_\infty[AlSiO_5^{3-}]$ aluminosilicate sheet explicitly neglects the "atomic-size" effect and focuses on the electronegativity perturbation.

Since the tetrahedral bond lengths and the orbital exponents are the same in $^2_\infty[Si_2O_5^{2-}]$ and $^2_\infty[AlSiO_5^{3-}]$, all overlap integrals, S_{ij}, are the same in both sheets. The *only* difference between $^2_\infty[Si_2O_5^{2-}]$ and $^2_\infty[AlSiO_5^{3-}]$ is that the atomic orbitals of half of the tetrahedral atoms have the VOIE's of silicon and half the VOIE's of aluminum. Though the band structure of $^2_\infty[AlSiO_5^{3-}]$ clearly resembles that of $^2_\infty[Si_2O_5^{2-}]$, all bonding bands of the former are narrower and their centers of gravity lie higher in energy than the latter (Figures 3 and 4). The reason the bands lie at higher energies is that even though these valence bands are primarily on oxygen, they nevertheless have small Si and Al contributions. The Al admixture is less stabilizing (higher H_{ii}) than the Si.

The bandwidth effect makes an interesting point. Usually it is said that bandwidth depends on overlap between unit cells.[44] But that is the same for Si and **Al**. Actually, the bandwidth depends on the energy matrix element between unit cells, H_{ij}, rather than S_{ij}. In the extended Hückel formalism H_{ij} is proportional to S_{ij} but also the the diagonal matrix element H_{ii}, and so is smaller for **Al** than Si.

Finally, the band structure of the $^2_\infty[AlSiO_5^{3-}]$ (layer-group symmetry *p3m1*) tetrahedral sheet appears in Figure 5. In this latter aluminosilicate sheet, all tetrahedra have $\bar{4}3m$ point symmetry but silicate and aluminate tetrahedral-bond lengths are different (*d*(Al–O) = 1.748 Å, *d*(Si–O) = 1.618 Å). Al now differs from Si in both orbital energies and exponents.

The band structure of $^2_\infty[AlSiO_5^{3-}]$ (Figure 5) is not profoundly different from that of $^2_\infty[Si_2O_5^{2-}]$ or $^2_\infty[AlSiO_5^{3-}]$ (Figures 3 and 4). Thus, we can represent the perturbation that results when $Al(III)_{tet}$ substitutes for $Si(IV)_{tet}$ as arising essentially from the electronegativity difference between aluminum and silicon. The "bonding" bands become narrower and shift to higher energies. These changes in the band structure are consistent with experimental Si Kβ XES spectra. The "nonbonding" bands are essentially uneffected by $Al(III)_{tet} \rightarrow Si(IV)_{tet}$ substitution.

The crystal orbitals of the eight lowest states at $\mathbf{k}_\Gamma = [0, 0]$, the center of the Brillouin zone, are illustrated in Figure 6a for $^2_\infty[Si_2O_5^{2-}]$ (layer-group symmetry *p6mm*). The corresponding states for $^2_\infty[AlSiO_5^{3-}]$ (layer-group symmetry *p3m1*) are shown in Figure 6b. Although our illustrations in Figure 6 show what appears to be $[Si_2O_7^{4-}]$, we are actually dealing with the repeat unit $[Si_2O_5^{2-}]$. These states clearly resemble one another. The changes that occur when $Al(III)_{tet} \rightarrow Si(IV)_{tet}$ in $^2_\infty[AlSiO_5^{3-}]$ are primarily due to an electronegativity perturbation. Minor differences in the appearance of the states illustrated in Figure 6 arise from the mixing of states, which in *p6mm* was forbidden but in *p3m1* is allowed.

III. Population Analysis of Aluminosilicate Tetrahedral Sheets. The gross atomic charges (nuclear charge minus the atomic population) for the atoms in several tetrahedral sheets are given in Table I. Table II shows the distribution of excess charge relative to $^2_\infty[Si_2O_5^{2-}]$ (layer-group symmetry *p6mm*) for atoms

Table I. Gross Atomic Charges (Nuclear Charges minus Atomic Populations) in Idealized, Isolated Aluminosilicate Tetrahedral Sheets

	tetrahedral sheet			
atom	$^2_\infty[Si_2O_5^{2-}]$	$^2_\infty[AlSiO_5^{3-}]$	$^2_\infty[AlSiO_5^{3-}]$	$^2_\infty[AlSi_3O_{10}^{5-}]$
Si	+2.47	+2.41	+2.42	+2.45
Al		+1.95	+2.13	+2.13
O_{apical}				
O[–Si]	−1.61	−1.61	−1.61	−1.61
O[–Al]		−1.72	−1.75	−1.75
O_{basal}				
O[(–Si)$_2$]	−1.24			−1.24
O[–Al,–Si]		−1.35	−1.40	−1.40

Table II. Excess Negative Charge Distribution of Isolated, Idealized Aluminosilicate Tetrahedral Sheets Relative to $^2_\infty[Si_2O_5^{2-}]$ (Layer-Group Symmetry *p6mm*)

	tetrahedral sheet		
atom	$^2_\infty[AlSiO_5^{3-}]$	$^2_\infty[AlSiO_5^{3-}]$	$^2_\infty[AlSi_3O_{10}^{5-}]$
Si	−0.06	−0.05	−0.02
Al	−0.52	−0.34	−0.34
O_{apical}			
O[–Si]	+0.00	−0.00	−0.00
O[–Al]	−0.11	−0.14	−0.14
O_{basal}			
O[(–Si)$_2$]			−0.00
O[–Al,–Si]	−0.11	−0.16	−0.16

(45) Vainshtein, B. K. *Modern Crystallography*; Springer-Verlag: New York, 1981; Vol. I, pp 118–121.

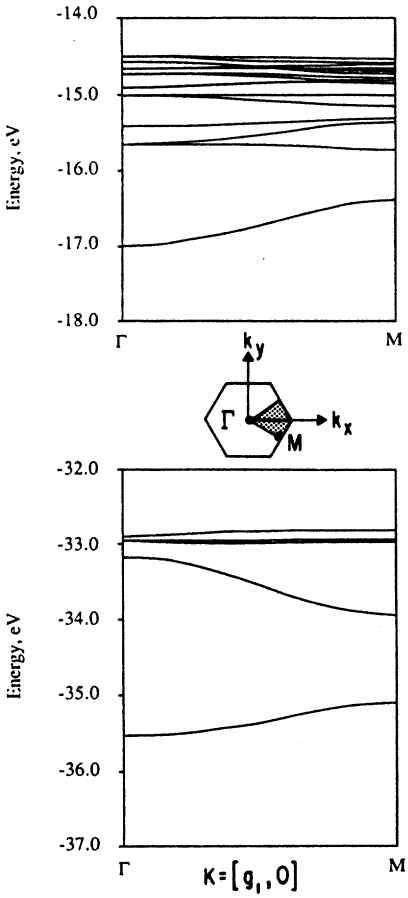

Figure 4. Band structure of a hypothetical $^2_\infty[AlSiO_5^{3-}]$ tetrahedral sheet (layer group $p3m1$) from $\mathbf{k}_\Gamma$ to $\mathbf{k}_M$ showing the first Brillouin zone with irreducible wedge (shaded), symmetry points, and lines.

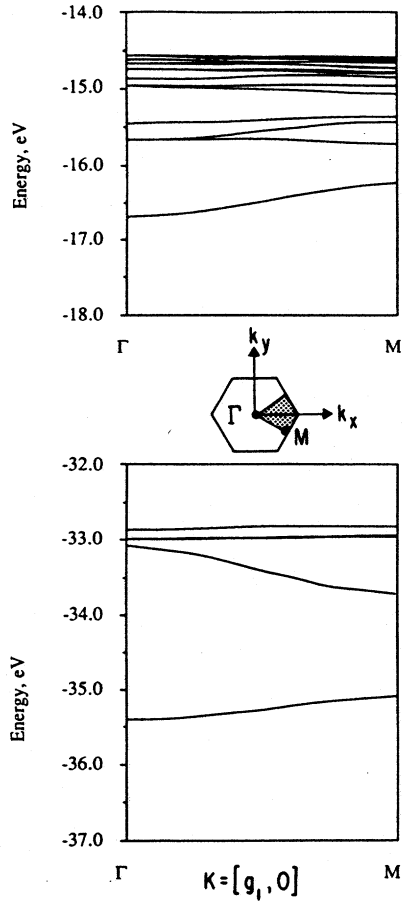

Figure 5. Band structure of the idealized $^2_\infty[AlSiO_5^{3-}]$ tetrahedral sheet (layer group $p3m1$) from $\mathbf{k}_\Gamma$ to $\mathbf{k}_M$ showing the first Brillouin zone with irreducible wedge (shaded), symmetry points, and lines.

in $^2_\infty[AlSiO_5^{3-}]$ (layer-group symmetry $p3m1$), $^2_\infty[AlSiO_5^{3-}]$ (layer-group symmetry $p3m1$), and $^2_\infty[AlSi_3O_{10}^{5-}]$ (layer-group symmetry $p6mm$). Each silicate tetrahedron in $^2_\infty[AlSi_3O_{10}^{5-}]$ (layer-group symmetry $p6mm$) is linked to two other silicate tetrahedra and one aluminate tetrahedron (Figure 2b). Half of the $^2_\infty[AlSi_3O_{10}^{5-}]$ basal oxygens form [Si–O–Al] bridges, and half, [Si–O–Si] bridges.

We can see that a picture significantly different from a strictly electrostatic-bonding model emerges when orbital interactions are allowed. $Al(III)_{tet} \rightarrow Si(IV)_{tet}$ deposits −0.34 unit of excess charge (as a positive charge deficit) at the substitution site in $^2_\infty[AlSiO_5^{3-}]$. Excess negative charge is deposited on the oxygens directly bonded to the aluminum (viz., −0.14 and −0.16 unit per atom). The apical oxygen receives most of the excess negative charge, as we would expect. Finally, a small excess negative charge of about −0.05 unit per atom is deposited on the next-nearest-neighbor silicon atoms.

Over just how extensive a region the excess negative charge is deposited can be seen by comparing $^2_\infty[AlSiO_5^{3-}]$ and $^2_\infty[AlSi_3O_{10}^{5-}]$. The excess negative charge on the substitution site and the nearest-neighbor oxygens is the same in these two aluminosilicate tetrahedral sheets. The only difference is found on the next-nearest-neighbor silicon atoms. Recall that in $^2_\infty[AlSiO_5^{3-}]$ each silicon is surrounded by *three* aluminum atoms, while in $^2_\infty[AlSi_3O_{10}^{5-}]$ each silicon has *one* aluminum and two silicon neighbors (Figure 2). Thus, each silicon in $^2_\infty[AlSi_3O_{10}^{5-}]$ should receive about one-third of the excess negative charge in $^2_\infty[AlSiO_5^{3-}]$.

The density of states, DOS, is defined such that DOS(E) dE ≡ number of states between E and E + dE. It gives us an energy distribution of electronic states. We can partition the DOS into contributions by atoms, orbitals, or combinations thereof. This is commonly referred to as "projections of the DOS" and represents the energy distribution of an atom or orbital contribution to the crystal orbitals. Integration overal all occupied states yields the total electron density on a given atom or in a specified atomic orbital.

Table III. Integrated Crystal Orbital Overlap Populations of Tetrahedral Bonds in Idealized Aluminosilicate Tetrahedral Sheets

bond	tetrahedral sheet			
	$^2_\infty[Si_2O_5^{2-}]$	$^2_\infty[AlSiO_5^{3-}]$	$^2_\infty[AlSiO_5^{3-}]$	$^2_\infty[AlSi_3O_{10}^{5-}]$
$Si–O_a$	0.54	0.54	0.54	0.54
$Si–O_b$[–Si]	0.50			0.50
$Si–O_b$[–Al]		0.52	0.52	0.52
$Al–O_a$[a]		0.43		
$Al–O_b$[–Si][a]		0.38		
$Al–O_a$[b]			0.39	0.39
$Al–O_b$[–Si][b]			0.31	0.31

[a] Overlap populations in Al–O and Si–O bonds can be compared to one another because bond lengths and orbital exponents are the same. [b] Al–O bonds can be compared to one another, but overlap populations in Al–O and Si–O bonds cannot.

The projected DOS curves for the 3s and 3p orbitals of aluminum and silicon in $^2_\infty[Si_2O_5^{2-}]$ (layer-group symmetry $p6mm$) and $^2_\infty[AlSiO_5^{3-}]$ (layer-group symmetry $p3m1$) appear in Figure 7. Mixing of next-nearest-neighbor aluminum and silicon orbitals can be clearly seen in the projected DOS curves for Al(3s) and Si(3s), Si(3s) dominating in the band at −35.2 eV and Al(3s) dominating in the −33.7-eV band. As in $^2_\infty[Si_2O_5^{2-}]$, the −33-eV peak involves cation 3p to O(2s) bonding and there is substantial cation 3s–3p mixing in the "O(2p)" bands.

Atomic size and bond length notwithstanding, the difference in electronegativity is a major reason the Al–O bond is weaker than the Si–O bond. The overlap populations of $Si–O_{basal}$[–Al] bonds (Table III), and hence their strength, increase in silicate tetradedra *directly* linked to aluminate tetrahedra. The overlap population in $Si–O_{basal}$[–Si] bonds are the same in $^2_\infty[AlSi_3O_{10}^{5-}]$ and $^2_\infty[Si_2O_5^{2-}]$, indicating that the perturbation associated with this isomorphous substitution is confined to the tetrahedron in which the substitution occurs, the $Si–O_{basal}$[–Al] bonds and the

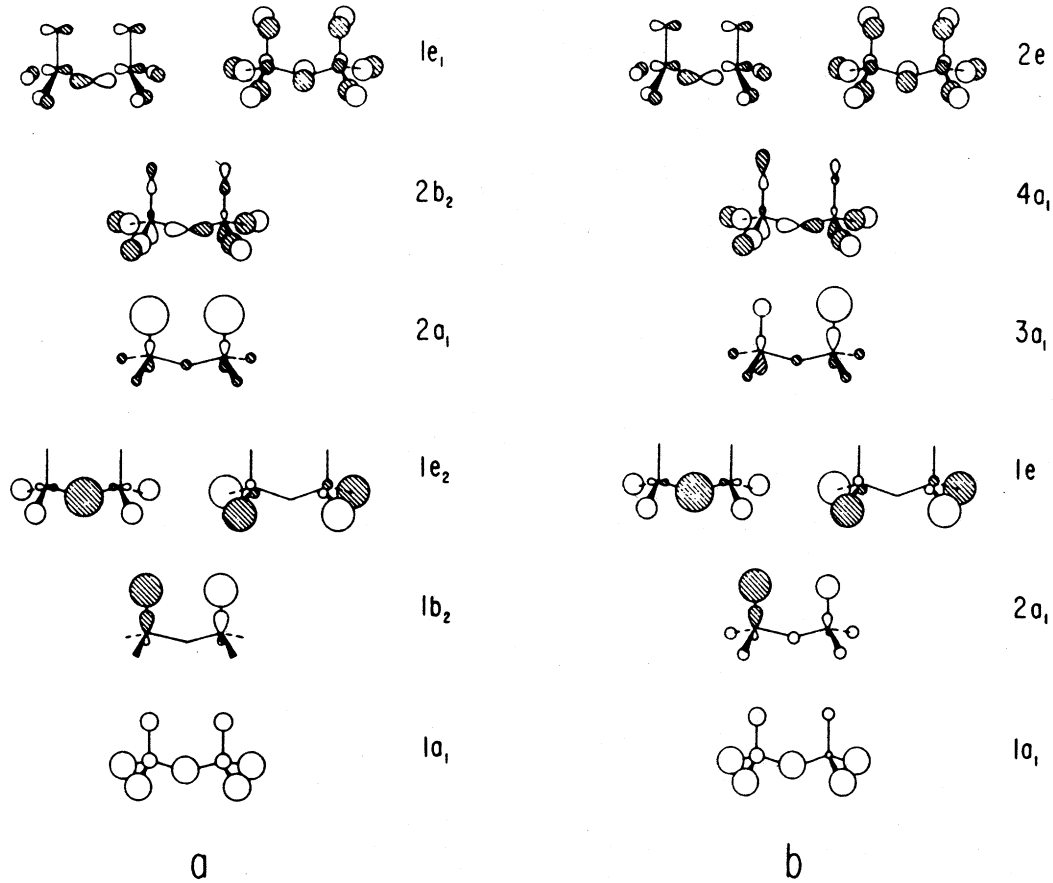

Figure 6. Bonding orbitals at $\mathbf{k}_\Gamma$, the center of the Brillouin zone, for (a) the ${}^2_\infty[Si_2O_5^{2-}]$ tetrahedral sheet (layer group *p6mm*) and (b) the ${}^2_\infty[AlSiO_5^{3-}]$ tetrahedral sheet (layer group *p3m*1).

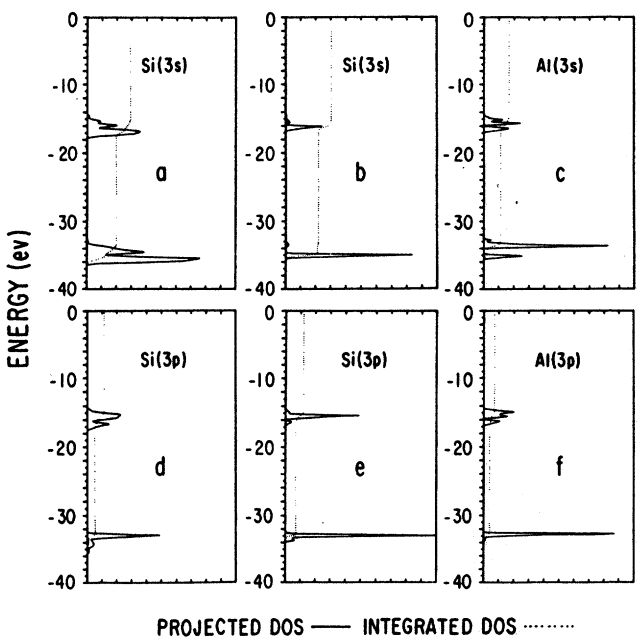

Figure 7. Projected density of states: (a) Si(3s) of ${}^2_\infty[Si_2O_5^{2-}]$ (layer group *p6mm*); (b) Si(3s) of ${}^2_\infty[AlSiO_5^{3-}]$ (layer group *p3m*1); (c) Al(3s) of ${}^2_\infty[AlSiO_5^{3-}]$ (layer group *p3m*1); (d) Si(3p) of ${}^2_\infty[Si_2O_5^{2-}]$ (layer group *p6mm*); (e) Si(3p) of ${}^2_\infty[AlSiO_5^{3-}]$ (layer group *p3m*1); (f) Al(3p) of ${}^2_\infty[AlSiO_5^{3-}]$ (layer group *p3m*1).

silicon of silicate tetrahedra directly linked to the site of substitution. The bonding in the aluminate tetrahedra is the same in ${}^2_\infty[AlSi_3O_{10}^{5-}]$ and ${}^2_\infty[AlSiO_5^{3-}]$, indicating that the Al:Si ratio has essentially no effect on aluminate bonding.

A bond order or bond strength index is essential in a chemical approach to bonding. In molecular orbital theory the most useful index of this kind has proven to be the Mulliken overlap population.[25,26] The overlap population associated with a specific contact in a solid can be evaluated by weighting the "DOS(E) dE" by the overlap population of all states in the interval E to E + dE. This is referred to as a "crystal orbital overlap population" (COOP) curve.[46] A COOP curve for a given contact permits us to evaluate over which energy intervals bonding interactions dominate, similarly for antibonding interactions.

The COOP curves for Si–O and Al–O bonds in ${}^2_\infty[Si_2O_5^{2-}]$ (layer-group symmetry p6mm) and ${}^2_\infty[AlSiO_5^{3-}]$ (layer-group symmetry *p3m*1) are shown in Figure 8. The differences between Si–O bonding and Al–O bonding, while not substantial, are most apparent in the lower two peaks of the "O(2s)" band involving [Al(3s),Si(3s)]–O(2s) bonding. Mixing of aluminum and silicon orbitals is lowest in these regions, reflecting the projected DOS for Al(3s) and Si(3s) mentioned above. The main point to be made from these COOP curves is that Al–O bonding and Si–O bonding are not substantially different and bonding interactions involving O(2s) orbitals are as important as those between cation and O(2p) orbitals in aluminosilicate tetrahedral sheets.

Earlier, we suggested that the lowest eight bands in either ${}^2_\infty[Si_2O_5^{2-}]$ or ${}^2_\infty[AlSiO_5^{3-}]$ could be thought of as the "bonding" bands. Justification for this qualitative assignment can be found by comparing the COOP curves shown in Figure 8 and the band-structure diagrams of Figures 3 and 5. Most of the bonding overlap is found at energies covered by the eight lowest bands.

IV. Population Analysis of Isomorphous Substitution in the Octahedral Sheet of 2:1 Phyllosilicates. We performed calculations on two idealized single-layer structures of the type illustrated in Figure 1. The first of these is an idealized pyrophyllite, ${}^2_\infty[Al_2(OH)_2(Si_2O_5)_2]$ (layer-group symmetry *c*2/*m*), and the second a hypothetical celadonite, ${}^2_\infty[MgAl(OH)_2(Si_2O_5)_2^-]$ (layer-group symmetry *p*121). All M–O bond lengths for the "octahedral" cations (the coordination polyhedral are actually trigonal antiprisms) in both layers are equal at 1.924 Å. Further details of

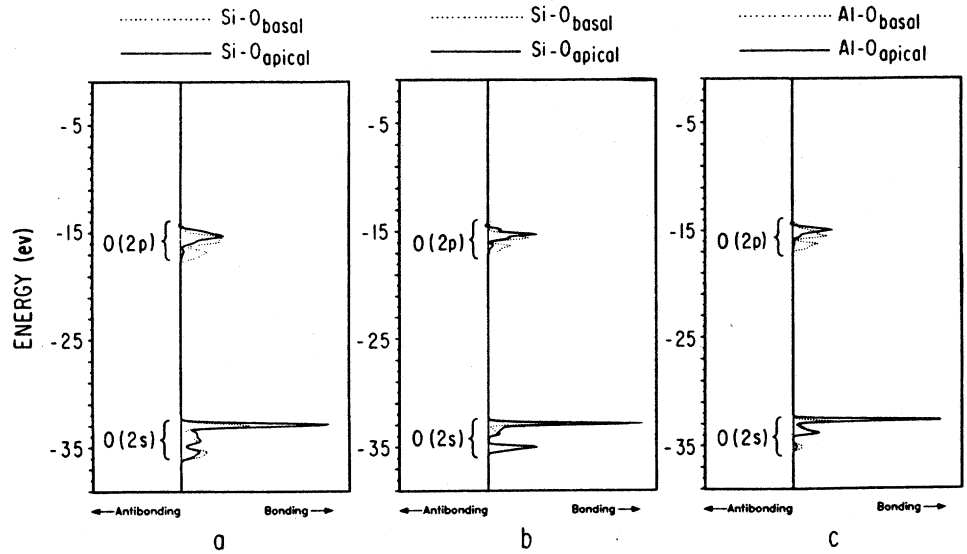

Figure 8. Crystal orbital overlap population curves: (a) Si–O_{basal} (solid line) and Si–O_{apical} (dashed line) bonds of $^2{}_\infty[Si_2O_5^{2-}]$ (layer group *p6mm*); (b) Si–O_{basal} (dashed line) and Si–O_{apical} (solid line) bonds of $^2{}_\infty[AlSiO_5^{3-}]$ (layer group *p3m1*); (c) Al–O_{basal} (dashed line) and Al–O_{apical} (solid line) bonds of $^2{}_\infty[AlSiO_5^{3-}]$ (layer group *p3m1*).

Table IV. Gross Atomic Charges (Nuclear Charges minus Atomic Populations) in Idealized Pyrophyllite, $^2{}_\infty[Al_2(OH)_2(Si_2O_5)_2]$, and Celadonite, $^2{}_\infty[\mathbf{Mg}Al(OH)_2(Si_2O_5)_2^-]$, and the Excess Charge Distributions Resulting from $Mg(II)_{oct} \rightarrow Al(III)_{oct}$

	phyllosilicate		
atom	pyrophyllite	celadonite	excess charge
Si	+2.49	+2.48	−0.01
Al	+2.28	+2.12	−0.16
Mg		+1.86	−0.42
O_{apical}	−1.39	−1.42	−0.03
$O_{hydroxyl}$	−1.15	−1.26	−0.11
O_{basal}	−1.25	−1.26	−0.01

the symmetry and structure for these layers can be found in the Appendix. The only difference between $^2{}_\infty[Al_2(OH)_2(Si_2O_5)_2]$ and $^2{}_\infty[\mathbf{Mg}Al(OH)_2(Si_2O_5)_2^-]$ is that in the latter layer structure half of the aluminum atoms have been replaced by pseudo-magnesium atoms, **Mg**, whose orbital VOIE's are those generally assigned to magnesium but whose orbital exponents are those generally assigned to aluminum in extended Hückel calculations (Table VI). This latter approach allows us to compare the overlap populations of Mg–O and Al–O in these two structures and how they are affected solely by the electronegativity perturbation of replacing an atom with one set of VOIE's by another with different VOIE's.

The computed ionic charges and the excess charge distributions for $^2{}_\infty[Al_2(OH)_2(Si_2O_5)_2]$ (layer-group symmetry *c2/m*) and $^2{}_\infty[\mathbf{Mg}Al(OH)_2(Si_2O_5)_2^-]$ (layer-group symmetry p121) appear in Table IV. Overlap populations for certain contacts in these layers are given in Table V. As in the case of $Al(III)_{tet} \rightarrow Si(IV)_{tet}$, some of the excess negative charge is found at the substitution site. Unlike the tetrahedral substitution case, however, more of the excess negative charge is deposited on the next-nearest-neighbor aluminum atoms and less on the nearest-neighbor oxygen atoms directly coordinating the magnesium. Excess negative charge at the cation sites is actually a deficit of positive charge at that location.

The picture that emerges from this analysis is that about half of the excess charge associated with the $Mg(II)_{oct} \rightarrow Al(III)_{oct}$ substitution appears as a positive charge deficit at the substitution site. Sixteen percent of the remaining excess charge is deposited at the next-nearest-neighbor aluminum atoms as a deficit of positive charge. Overlap populations show that Al–O bonds are strengthened by the substitution.

We must explain the dramatic difference in excess negative charge distributions arising from tetrahedral ($Al(III)_{tet} \rightarrow Si(IV)_{tet}$) and octahedral ($Mg(II)_{oct} \rightarrow Al(III)_{oct}$) substitution. A clue to this mystery can be found in our extended Hückel, tight-binding analysis of orbital interactions in lizardite, $^2{}_\infty[Mg_3(OH)_4(Si_2O_5)]$ (layer-group symmetry *p31m*), and talc, $^2{}_\infty[Mg_3(OH)_2(Si_2O_5)_2]$ (layer-group symmetry *c2/m*), where we found that there is essentially no orbital interaction between magnesium and the tetrahedral sheet(s) or hydroxyls.[7] There are two possible consequences of $Mg(II)_{oct} \rightarrow Al(III)_{oct}$ substitution: (a) *all* of the excess negative charge will remain at the substitution site as a positive charge deficit or (b) orbital interactions between magnesium and next-nearest-neighbor aluminum atoms will deposit some of the excess charge on the aluminum atoms.

Table V. Integrated Crystal Orbital Overlap Populations for Tetrahedral and Octahedral Bonds in Idealized Pyrophyllite, $^2{}_\infty[Al_2(OH)_2(Si_2O_5)_2]$, and Celadonite, $^2{}_\infty[\mathbf{Mg}Al(OH)_2(Si_2O_5)_2^-]$

	phyllosilicate			phyllosilicate	
bond	pyro-phyllite	cela-donite	bond	pyro-phyllite	cela-donite
Si–O_{apical}	0.52	0.54	Al–$O_{hydroxyl}$	0.23	0.29
Si–O_{basal}	0.51	0.50	**Mg**–O_{apical}		0.11
Al–O_{apical}	0.19	0.22	**Mg**–$O_{hydroxyl}$		0.02

The transfer of excess charge, via orbital interactions, from magnesium to next-nearest-neighbor aluminum atoms in the octahedral sheet is a reasonable phenomenon. The dependence of Si Kβ XES spectra on $Al(III)_{tet} \rightarrow Si(IV)_{tet}$ substitution in aluminosilicates[17,22,23] is persuasive evidence that orbital mixing occurs between next-nearest-neighbor aluminum and silicon atoms in tetrahedral frameworks. A similar shift occurs in the Al Kβ XES spectra of cordierite, $[Mg_2Al_4Si_5O_{18}]$, relative to those of the feldspars anorthite, $[CaAl_2Si_2O_8]$, and microcline, $[KAlSi_3O_8]$.[47] Of course, a better test of our contention would be found by comparing both the Al Kβ shift in celadonite relative to that in pyrophyllite and the Al photoelectron binding energies.

Next-nearest-neighbor distances are identical for tetrahedral and octahedral cations in phyllosilicates. Given the fact that the orbital exponents of magnesium valence orbitals are larger than those of aluminum and both are larger than those of silicon, we can conclude that the overlap integrals for $Mg(II)_{oct}$–$Al(III)_{oct}$ contacts will be larger than those for $Al(III)_{tet}$–$Si(IV)_{tet}$ contacts.

Summary

If the substituting atom in a silicate framework is less electronegative than silicon (e.g., aluminum), the T–O bonds surrounding the substituting atom will lengthen and the Si–O[–T] bonds in corner-sharing tetrahedra will shorten. The atomic

Dodd, C. G.; Glenn, G. L. *Am. Mineral.* **1969**, *54*, 1299.

Table VI. Orbital Parameters Used in the Extended Hückel Calculations

atom	orbital	VOIE, eV	exponent
Al	3s	−12.3	1.167
	3p	−6.5	1.167
Al	3s	−12.3	**1.383**
	3p	−6.5	**1.383**
Mg	3s	−9.0	0.950
	3p	−4.5	0.950
Mg	3s	−9.0	**1.167**
	3p	−4.5	**1.167**
O	2s	−32.3	2.275
	2p	−14.8	2.275
Si	3s	−17.3	1.383
	3p	−9.2	1.383
H	1s	−13.6	1.300

Table VII. First Brillouin Zone Symmetry Points and Lines[a]

layer-group symmetry	$\mathbf{k}_\Gamma$	$\mathbf{k}_K$	$\mathbf{k}_M$	$\mathbf{k}_{\Delta(\Gamma K)}$	$\mathbf{k}_{\Sigma(\Gamma M)}$	$\mathbf{k}_{T(MK)}$
p6mm	*6mm*	*3m*	*2mm*	*m*	*m*	*m*
p3m1	*3m*	1	*m*	1	*m*	1

[a] Reciprocal space basis vectors: $\mathbf{g}_1 = (2\pi/a\sqrt{3}, -2\pi/a)$ and $\mathbf{g}_2 = (4\pi/a\sqrt{3}, 0)$. $\mathbf{k}_\Gamma = [0, 0]$; $\mathbf{k}_K = [{}^2/_3, {}^1/_3]$; $\mathbf{k}_M = [{}^1/_2, 0]$; $\mathbf{k}_{\Delta(\Gamma K)} = [2\alpha, \alpha]$, $0 < \alpha < {}^1/_3$; $\mathbf{k}_{\Sigma(\Gamma M)} = [\beta, 0]$, $0 < \beta < {}^1/_2$; $\mathbf{k}_{T(MK)} = [{}^1/_2 + \gamma, 2\gamma]$, $0 < \gamma < {}^1/_6$.

populations of the nearest-neighbor and, to a much lesser extent, next-nearest-neighbor atoms will increase. The opposite effects will occur if the substituting atom is more electronegative (e.g., phosphorus). Excess negative charge deposited on the framework when the substituting atom has a lower nuclear charge than silicon will be partitioned between the site of the substituting atom and its nearest-neighbor oxygens. The perturbation will largely be restricted to the TO_4Si_x (x = 3 or 4) unit because nearest-neighbor orbital interactions are so strong.

Technically, the octahedral sites in phyllosilicates are extra-framework sites. Coulombic interactions between the substituting atom and oxygens in the octahedral sheet can dominate orbital interactions without jeopardizing the structure of phyllosilicates. Orbital interactions between magnesium and oxygen are negligible. When magnesium replaces aluminum in the octahedral sheet of dioctahedral montmorillonites or celadonite, next-nearest-neighbor magnesium–aluminum interactions represent the only means of displacing electron density away from the substitution site. The excess negative charge displaced from the substitution site bypasses nearest-neighbor oxygens and is deposited on next-nearest-neighbor aluminum. Shifts in the Al Kβ transition in response to aluminum substitution by magnesium are taken as evidence that next-nearest-neighbor interactions are possible. A decrease in the binding energy of photoelectrons ejected from aluminum in a magnesium-rich celadonite would provide a further test of the hypothesis that most of the displaced charge resides on the next-nearest-neighbor aluminum atoms.

Acknowledgment. R.H. is grateful to the National Science Foundation for its support of this work through Research Grant CHE 8406119. W.B. is grateful to the Cornell Chapter of Sigma Xi for its early support of this study under its Grants-in-Aid Program.

Appendix

The orbital parameters used in our extended Hückel, tight-binding calculations appear in Table VI. The important distances used in our calculations are d(Si–O) = 1.618 Å,[4] $d(Al_{tet}–O)$ = 1.748 Å,[4] $d(Al_{oct}–O)$ = 1.924 Å (mean $d(Al_{oct}–O)$[48]), d(Mg–O) = 2.067 Å (mean d(Mg–O)[49]), d(O–H) = 0.971 Å (d(H–O)[48]), $d(O–O)_{Mg}$ (shared-edge) = 2.430 Å, and $d(O–O)_{Al}$ (shared-edge) = 2.567 Å. The 4-fold oxygen polyhedra coordinating silicon or aluminum have point symmetry $\bar{4}3m$, while coordination polyhedra for both magnesium and aluminum have point symmetry $3m$. The octahedral sheet has layer-group symmetries $c2/m$ in pyrophyllite and $c121$ in celadonite. The ${}^2_\infty[Si_2O_5^{2-}]$, tetrahedral sheet has layer-group symmetry $p3m1$ pyrophyllite and celadonite.

A set of 24 k-points for the $p6mm$ layer group, a set of 44 k-points for the $p3m1$ layer group, and a set of 16 k-points for the $c121$ and $c2/m$ layer groups were used in the irreducible wedges of the first Brillouin zones.[50] Density-of-state and COOP calculations, which require integration over the first Brillouin zone, were based on these special k-point sets. Since Cunningham did not include a k-point set for the trigonal lattice in his paper, we generated the k-point set for $p3m1$ by taking an irreducible wedge double that of $p6mm$ and using symmetry to generate the extra points in this new wedge from the smaller $p6mm$ set.

Registry No. Al, 7429-90-5; Mg, 7439-95-4.

(48) Lee, J. H.; Guggenheim, S. *Am. Mineral.* **1981**, *66*, 350.
(49) Mellini, M. *Am. Mineral.* **1982**, *67*, 587.
(50) Cunningham, S. L. *Phys. Rev. B: Solid State* **1974**, *10*, 4988.